SCIENTIFIC JOURNAL OF MARITIME RESEARCH [POMORSTVO]
University of Rijeka FACULTY OF MARITIME STUDIES

https://doi.org/10.31217/p.39.1.2

Automated Drag Optimization of a Torpedo Shaped AUV Using B-spline and Genetic Algorithm

Ibrahim Ayad[1,*], Nateche Tahar[1], Hamoudi Benameur[1], Cerdoun Mahfoudh[2], Hadj Meliani Mohammed[3], Mokhtari Abdellah[1]

[1] Aero-Hydrodynamic Naval Laboratory, Maritime Department, University of Sciences and Technology Mohammed Boudiaf USTO-MB, Oran, 31000, Algeria; e-mail: ibrahim.ayad@univ-usto.dz; abdellah.mokhtari@univ-usto.dz

[2] Laboratory of Fluid Mechanics, Military Polytechnical School, Bordj El Bahri, Algiers, 16046, Algeria; e-mail: cerdoun.mahfoudh@gmail.com

[3] LPTPM, Faculty of Technology, Hassiba BenBouali University of Chlef, Chlef, 02000, Algeria; e-mail: m.hadjmeliani@univ-chlef.dz

[*] Corresponding author

ARTICLE INFO

Original scientific paper
Received 16 October 2024
Accepted 20 November 2024

Key words:
AUV
Torpedo
Shape optimization
B-spline
Genetic algorithm
Drag reduction

ABSTRACT

Torpedo-shaped autonomous underwater vehicles (AUV) offer versatile capabilities such as surveying underwater environment, collecting data, performing inspections and even assisting in search and rescue operation. However, their design still attract the attention of manufacture due to the various parameters that affect the final shape. This article aims to optimize the shape of a torpedo-shaped (AUV) through the utilization of B-splines for shape representation and the application of genetic algorithms for form optimization, in which the main objective is to minimize the drag. The automated optimization procedure uses minimum control points to form the nose and the tail of the AUV whereas the cylindrical part remain unchanged. To evaluate the performance, the computational fluid dynamics (CFD) model as high fidelity model is used and it is calibrated for a DREA type UV. The overall strategy presents a drag reduction about 19%.

1 Introduction

The Autonomous Underwater Vehicles (AUVs) have become an indispensable tool in various industries, including oil and gas [1, 2], environmental monitoring [3], climate research [4], and cultural preservation [5]. These vehicles enable cost-effective and safe missions in harsh environments that would otherwise be difficult or impossible for humans to access. The design of the vehicle should allow for extended missions, requiring a long-lasting autonomy period that can span several months. As an illustration, it is not uncommon for scientific data collection missions in oceanography and climate research to extend up to 7 months [6].

Consequently, maximizing the operational potential of such vehicles has become imperative. This entails equipping them with as many tools as possible including propulsion systems, while also optimizing energy consumption and taking size constraints into account during the AUV design process. One solution for achieving better performance is to minimize water resistance. This is crucial because it directly affects the energy consumption of the propulsion system. One effective way to minimize resistance is to modify the shape of the AUV to make it more streamlined, resulting in less drag and better capability. In this context, numerous numerical investigations have been conducted to characterize and reduce the drag of AUVs.

Hess [7] developed an integral drag expression, employing it to assess drag efficiency across diverse body shapes. Sakar and al. [8] developed a cost-effective CFD method to simulate flow around axisymmetric AUVs, proving its numerical robustness and accuracy for efficient hull form design, significantly reducing early-stage design costs. Baker [9] proposed a methodology for simulating the flow around a standard bare submarine

hull. The emphasis is on creating a high-quality unstructured mesh for boundary layer flow resolution. Jagadeech and Murali [10] compared four low Reynolds number k-ε turbulence models for predicting hydrodynamic forces on underwater vehicle hull forms, with the k-ε AKN model consistently demonstrating superior performance in capturing flow characteristics. In another study, Jagadeech and al. [11] presented a towing tank-based experimental study on the hydrodynamic forces and moments acting on an autonomous underwater vehicle hull form, highlighting significant variations in coefficients with Reynolds number and angle of attack, providing valuable insights for efficient AUV guidance and control system design. Alvarez and al. [12] attempted to optimize the shape of an AUV operating near the free surface to minimize drag. They used a Rankine panel method and a simulated annealing algorithm. Karim and al. [13] introduced a 2D finite volume method, applying Reynolds-averaged Navier-Stokes equations, for computing viscous drag on various axisymmetric bodies, with different length-diameter ratios. The study incorporates structured and unstructured grids, testing various turbulence models. Alam and al. [14] introduced a flexible optimization framework utilizing non-dominated sorting genetic algorithm (NSGA-II) and infeasibility driven evolutionary algorithm (IDEA) to identify optimal designs for torpedo-shaped AUVs. de Sousa and al. [15] investigated turbulent flow over various Autonomous Underwater Vehicle hull configurations, aiming to identify a geometry that minimizes drag force, thereby enhancing energy efficiency and operational autonomy. Gao and al. [16] introduced a shape optimization platform for AUV hulls, emphasizing the use of a two-dimensional unstructured mesh, standard wall function, and adaptive mesh refinement to improve efficiency and accuracy, with the multi-island genetic algorithm (MIGA) proving superior to particle swarm optimization (PSO) in obtaining optimized hull shapes under general volume requirements, demonstrating the platform's robustness for AUV hull design. Mostafapour and al. [17] investigated the impact of Reynolds number on autonomous underwater vehicle hydrodynamics, utilizing computational fluid dynamics (CFD) and experimental validation. The results demonstrate that certain hydrodynamic parameters become Reynolds number-dependent, converging to a constant as Reynolds number increases. Sedini and al. [18] engaged a study that involves CFD model evaluation, calibration, and AUV optimization, demonstrating good agreement with experimental results and providing insights into added masses coefficients and damping force for understanding AUV acceleration behavior at sea. Saghafi and Lavimi [19] investigated the numerical analysis of flow around symmetrical autonomous underwater vehicles, aiming to decrease drag force by altering geometric shapes, particularly the noses and tails.

This study is part of an optimization perspective for developing a torpedo-shaped AUV with the aim of improving its hydrodynamic performance, such as drag. We began by proposing a model for constructing the geometry of the AUV. In contrast to the dominant geometry models in the literature, particularly mentioned in this introduction; which use Gertler [20] or Myring [21] equations, the adopted approach utilizes B-splines representation, widely used in various 'required geometry modeling' domains but underutilized in the AUV field. Next, a CFD study was conducted. The CFD model of the AUV was evaluated and calibrated based on the experimental works, realized by White [22] on DREA underwater vehicle. Once the CFD model validated, genetic algorithms were selected for the optimization process. Thus, a genetic algorithm (GA) was implemented and adapted to the problematic. Finally, we subsequently integrated the all (B-spline, CFD and GA) and built a fully automated optimization platform to find the best profile of the AUV with the minimum drag.

2 Geometry of the AUV

The design of the AUV is a torpedo shape. The vehicle model is axisymmetric and the geometry is constructed using two B-spline curves to represent the nose and the tail sections respectively C1 and C2, while the mid-section is a straight line to maintain the torpedo shape (Figure 1). B-spline curves are widely used in various applications, including computer graphics, CAD, animation, and industrial design. They are one of the most promising curves [23]. They offer a flexible and ef-

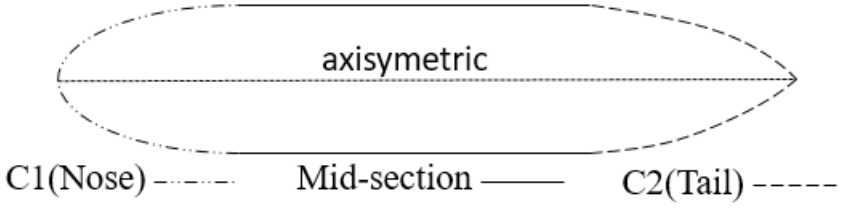

Figure 1 AUV Geometry

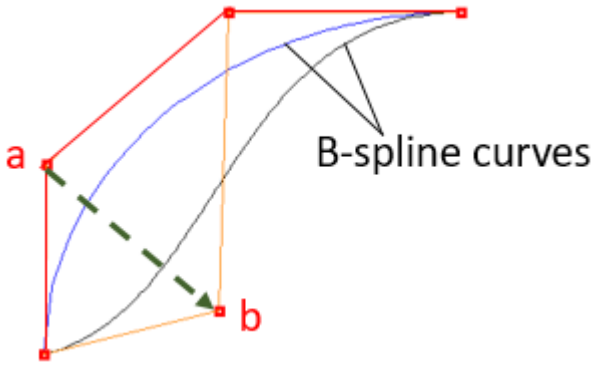

Figure 2 Changing geometry by moving one control point

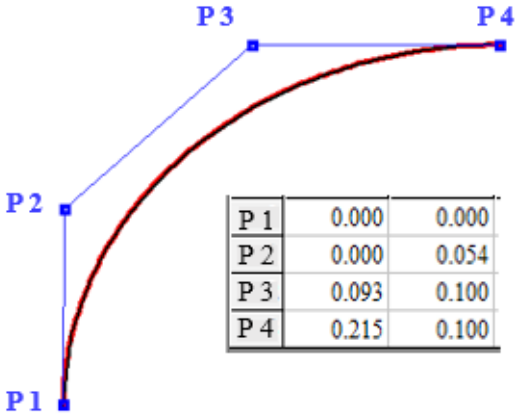

Figure 3 Matching an AUV's nose with a B-spline curve

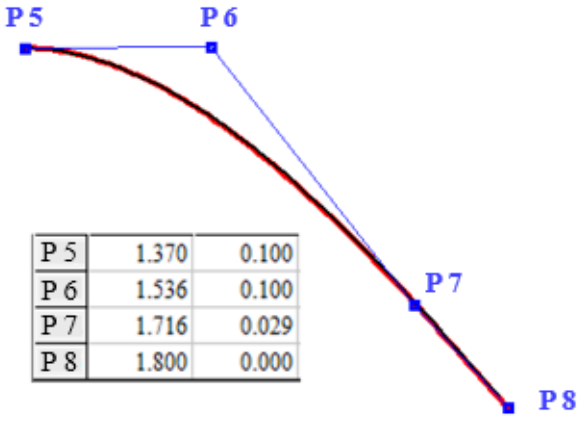

Figure 4 Matching an AUV's tail with a B-spline curve

ficient way to represent and manipulate smooth curves, making them a powerful tool in curve modeling and interpolation.

B-spline curves depend on their control points. The control points are points in space that influence the shape of the curve. By manipulating the positions of these control points, one can control the overall shape of the AUV geometry. Figure 2 Shows the change in geometry from the blue curve to the black one by simply moving one control point from position (a) to position (b).

2.1 B-spline [24]

The general formulation of a B-spline parametric curve $C(u)$ of degree p polynomial, defined by its related $(n + 1)$ points P_0, P_1, ..., and P_n (called control points) is:

$$C(u) = \sum_{i=0}^{n} N_{i,p}(u) P_i \quad (1)$$

where u is a parameter $(0 \le u \le 1)$.

$N_{i,p}$ are the B-spline basis functions defined as:

$$N_{i,0}(u) = \begin{cases} 1 & if\ u_i \le u < u_{i+1} \\ 0 & otherwise \end{cases} \quad (2)$$

$$N_{i,p}(u) = \frac{u-u_i}{u_{i+p}-u_i} N_{i,p-1}(u) + \frac{u_{i+p+1}+u}{u_{i+p+1}-u_{i+1}} N_{i,p-1}(u) \quad (3)$$

These functions are weight coefficients that serve to average control points to calculate a point of the curve that correspond to u.

$u_0 \le u_1 \le \cdots \le u_m$ define the knot vector $U = \{u_0, u_1, ..., u_m\}$.

Note that the number of knots $(m + 1)$, the degree of the basis functions p and the number of the basis functions (which represents the number of control points) n must satisfy the following relationship:

$$m = n + p + 1 \quad (4)$$

2.2 Geometry representation

In order to model the AUV torpedo shape, a B-spline of degree of 3 is chosen. This choice ensures $C^{(2)}$ continuity for the curves C1 and C2 [25]. As a consequence, this guarantees the tangent, the curvature and thus the machining path continuities [26]. The knot vector is a uniform vector that guarantees a clamped B-spline curve [27] passing through the first and last points. Based on the relationship between control points and knots (Equation 4), the minimum number of control points are selected, resulting in 4 control points. By setting the B-spline parameters in this way, curves of various UV torpedo shapes could be reproduced. By manipulating the control points, we were able to match several AUV's design geometries from literature that were based on different models, including Myring's and Gertler's. The flexibility of our approach allowed us to reproduce these diverse shapes by simply adjusting the positions of the control points. Figure 3 and Figure 4 are an example of matching optimized AUV by Sedini and al. [18] (in black) using B-spline curves (in red). P1, P2, P3, P4 are nose control points while P5, P6, P7, P8 are tail control points.

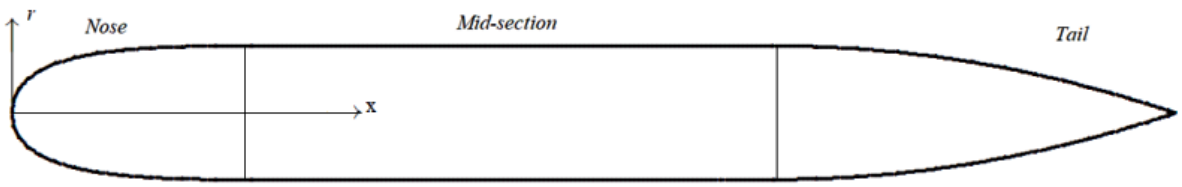

Figure 5 DREA UV

3 CFD model and evaluation

The reference geometry used to evaluate the appropriate mesh, CFD analysis and optimization process is a torpedo shaped UV bare hull named DREA (Project Defense Research Establishment Atlantic developed by Department of Research and Development Canada), that was experimentally realized by White [22].

3.1 Geometry of DREA UV

Geometric characteristics of DREA UV (Figure 5) are defined by mathematical equations (Equation 5, 6, 7) where l is the overall length and d is the maximum diameter, with $l/d = 8.75$.

For the nose: length 0.2 l

$$\frac{r_1(x)}{l} = \frac{d}{l}\left[2.56905\sqrt{\frac{x}{l}} - 3.48055\frac{x}{l} + \right.$$
$$\left. + 0.49848\left(\frac{x}{l}\right)^2 + 3.40732\left(\frac{x}{l}\right)^3\right], \quad 0 \le \frac{x}{l} \le 0.2. \tag{5}$$

For the mid-section: circular cylinder

$$\frac{r_2(x)}{l} = \frac{d}{2l}, \quad 0.2 \le \frac{x}{l} \le 1 - \frac{3d}{l}. \tag{6}$$

For the tail: length 3d

$$\frac{r_3(x)}{l} = \frac{d}{2l} - \frac{l}{18d}\left[\frac{x}{l} - \left(1 - \frac{3d}{l}\right)\right]^2, \quad 1 - \frac{3d}{l} \le \frac{x}{l} \le 1. \tag{7}$$

3.2 Turbulence model

The turbulence model used in this investigation is the K-Epsilon model [28], which is convenient for predicting the flow characteristics around the axisymmetric underwater vehicle and accurately capturing the behavior of the boundary layer [18, 29, 30]. The utilization of this model leads to results that consent with experimental data [19].

3.3 Domain and boundary conditions

The optimization process being proposed is an iterative computational procedure, which can become highly computationally expensive. Consequently, a decision has been made to employ a 2D mesh for the purposes of optimization. Rahul Krishna and al. [31] have shown that using a 2D simulation instead of a 3D one is an excellent alternative for similar CFD studies. The size and shape of the domain, as well as the positioning of inlet and outlet boundaries are selected to ensure flow recirculation avoidance. The dimensions of the domain and the positioning of the AUV are shown in Figure 6. L represents the length of the AUV and d its diameter.

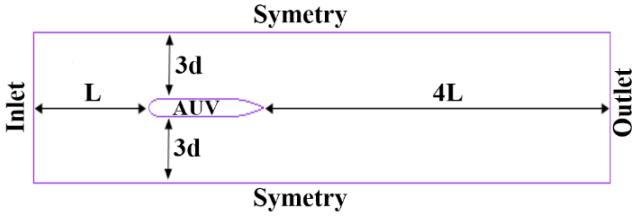

Figure 6 Computational domain

3.4 Mesh assessment

Selecting an unstructured mesh over a structured mesh is regarded as a beneficial choice in the construction of an optimization platform [16].

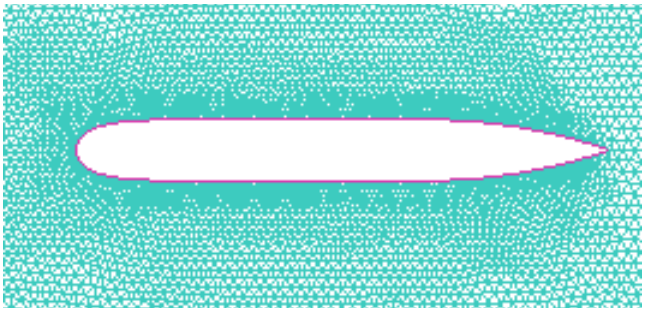

Figure 7 Unstructured Mesh

Due to the utilization of an unstructured mesh (Figure 7), the implementation of inflation layers on the surface of the geometry becomes necessary. These inflation layers help in resolving the velocity profile in the proximity of the wall, thereby enhancing the accuracy of predictions for wall shear stress.

For the CFD calculations, the thickness of the first layer is set based on Equation (8) [19].

$$\Delta y = L\,\Delta y^+ \sqrt{80}\,Re^{\frac{-13}{14}} \tag{8}$$

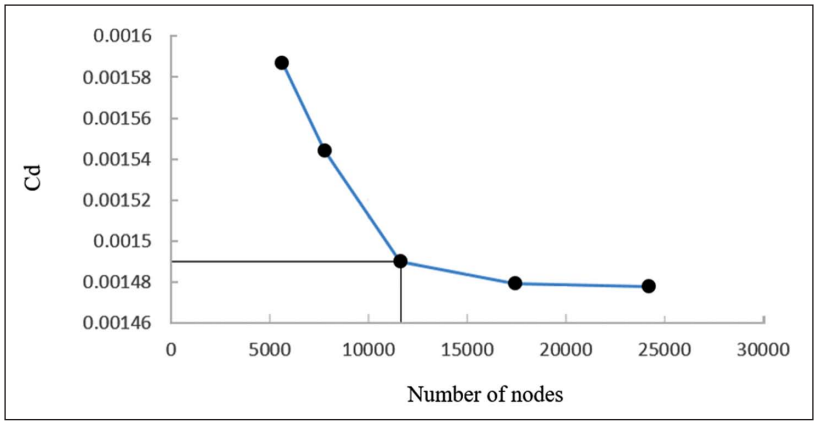

Figure 8 Effect of mesh size on drag coefficient

where: Δy is the thickness of the first mesh node, L is the length of the AUV, Δy^+ represents a non-dimensional distance from the wall to the first mesh node, Reynolds number.

In addition, 11 layers with a growth ratio of 1.1 were used. Mesh refinement was performed near the wall to ensure cell volume transition.

3.5 Mesh dependency

Mesh size independence tests are useful to achieve appropriate discretization with a minimal number of elements to reduce computation times without compromising result quality. The calculated drag coefficient for different sizes of the mesh made it possible to retain a total mesh size of 11616 nodes to perform our calculations (Figure 8).

3.6 Model evaluation

The evaluation of the mesh and the numerical model were performed based on the simulation of the experimental study realized by White [22]. This study was achieved on the axisymmetric bare hull named DREA. Table 1 shows a comparison between the experimental data, and the CFD results.

Table 1 shows that the obtained CFD drag coefficient results of the present study are in good agreement with the experimental data. The k-epsilon model is specifically efficient to target flows that concern the log-law region [32], where values of y+, as preference, should be optimally between 33 and 70. y+ is representative of the accuracy of the numerical predication [33]. Figure 9 shows that the y+ values for the discussed simulation are within acceptable suggested limits.

Table 1 Drag coefficient of DREA bare hull

$Re = 2.3\ 10^7$	Cd Experimental White [22]	Cd CFD Baker [9]	Cd CFD Karim [13]	Cd CFD (Present study)
Drag coefficient	0.00123 ± 0.000314	0.00167	0.00104	0.00149

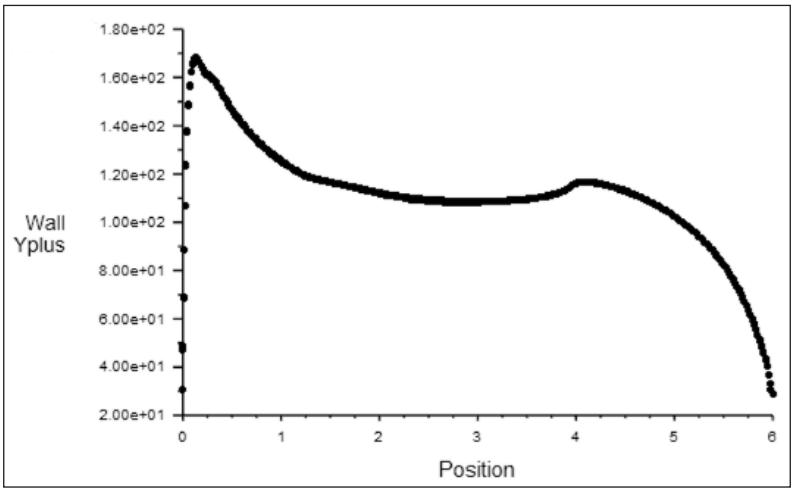

Figure 9 Values of y+ for DREA UV

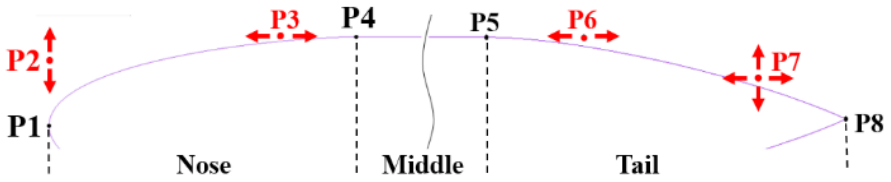

Figure 10 Optimization control points

4 Optimization of the AUV

The selected optimization parameter is the hydrodynamic drag coefficient Cd enabling the shape control. The geometric constraints that force the optimization process are to maintain the overall length of the torpedo shaped UV DREA; the length, the diameter and the positioning of its mid-section.

4.1 Optimization variables and objective function

Four control points P1, P2, P3 and P4 are used to define the shape of the nose, with P1 and P4 being fixed points. The other four control points P5, P6, P7 and P8 are employed to model the tail section, with P5 and P8 being fixed points (Figure 10). Consequently, P1 and P8 correspond respectively to the leading edge and the trailing edge, determining the overall length of the AUV. The straight line defined by P4 and P5 represents the mid-section, determining its length and the diameter of the AUV. P2, P3, P6 and P7 are optimization points, which are allowed to vary within their respective limit domains during the optimization process, ultimately converging towards an optimal solution. So a set of control points {P2, P3, P6, P7} called individual define a distinct shape of an AUV. This shape is calculated using B-spline.

4.2 Genetic algorithms

For the optimization process, we have opted for genetic algorithms. This class of stochastic population-based algorithms are known to be very robust algorithms, capable of converging towards the global optimum even when dealing with problems with complex objective functions. They harness the phenomena of evolution to iteratively unveil the optimal solution. This evolutionary mechanism relies on three key genetic operators: crossover, mutation, and selection [16].

The genetic algorithm steps (Figure 11) begins with an initial population composed of individuals that are all potential solutions. This population evolves through genetic operators. Crossover performs a mixture between individuals, favoring exploitation. Mutation introduces alterations, i.e., disturbances to the individuals, promoting exploration. Then, selection, which is a survival process, generates a new population that replaces

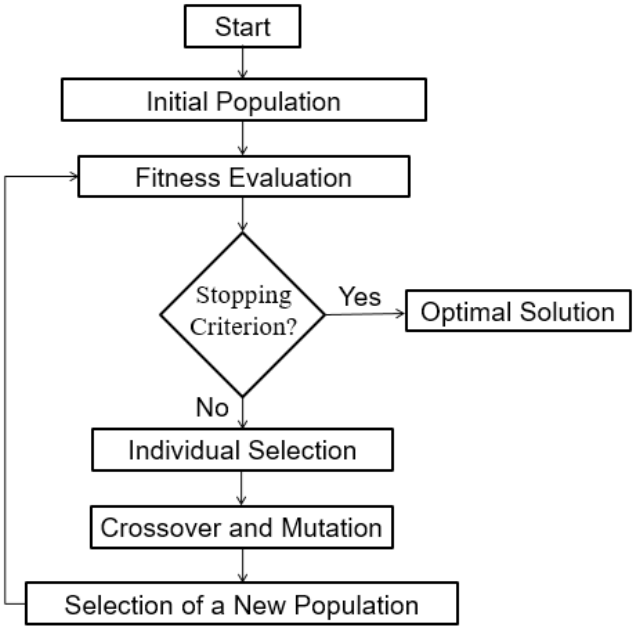

Figure 11 Genetic algorithm flowchart

the previous one. The survival of each individual depends on its fitness, which is determined by the objective function calculation. Finally, an optimal solution emerges as the result of this evolution.

The selected algorithm has been developed and tested on multiple benchmark functions [35, 36]. Then, it has been adapted for this study.

4.3 Optimization procedure

The flowchart of the fully automated optimization procedure is shown in Figure 12.

At the beginning, a population of N shape's candidates all considered as potential solutions is generated. Specifically, this is done by generating randomly N set of distinct control points {P1, P2, P6, P7}. Each shape's candidate is calculated using B-spline and related control points. Then, the drag is computed in batch-mode by utilizing predetermined journals ICEM and FLUENT. At this stage, N initial shape's candidates and their corresponding drags are obtained.

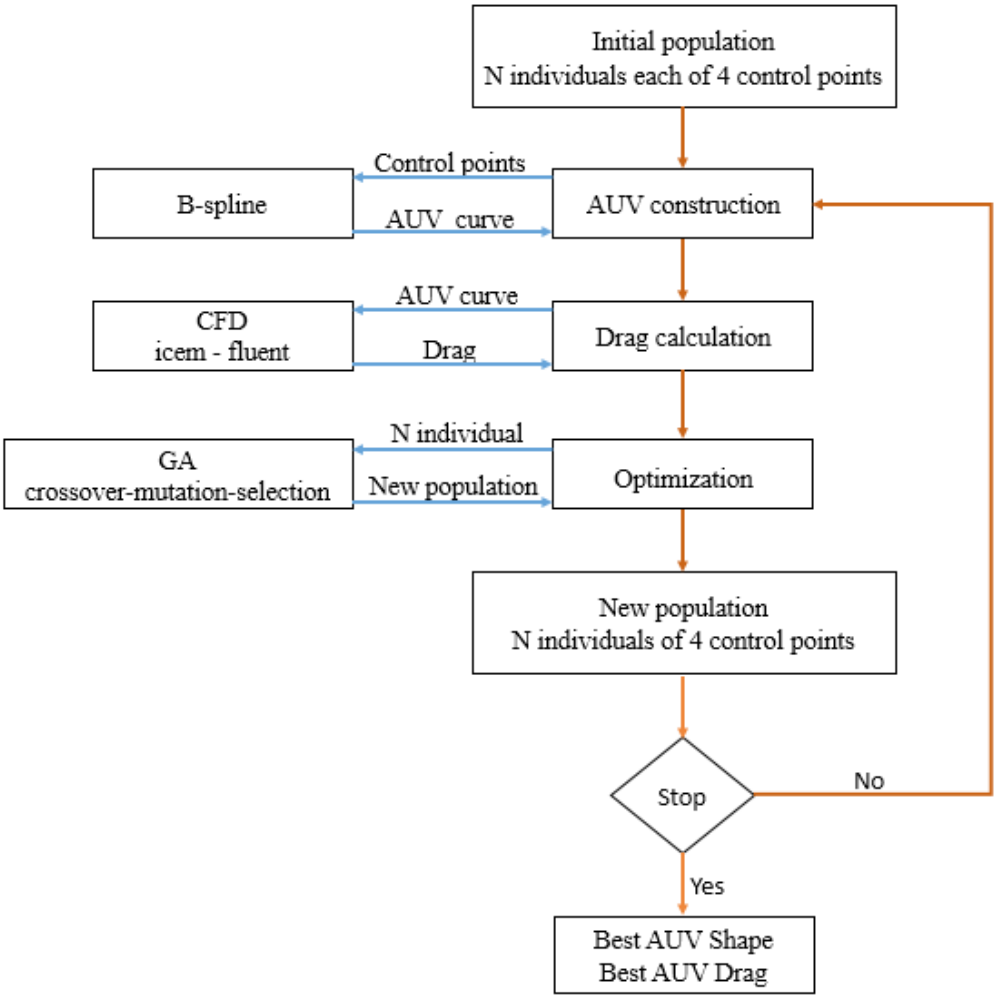

Figure 12 Fully automated optimization

The next step is to reproduce a new population of shape's candidates by manipulating the existing control points, and using the operators of the genetic algorithm. This is done by selecting randomly two individuals from the previous population, proportionally based on their fitness. Then applying genetic operators (crossover and mutation) during the reproduction. Once N new shape's candidates have been generated, they are evaluated in turn using B-spline, ICEM and FLUENT. The new generation of shape's candidates competes with the old one based on fitness. The most performant are then selected and integrated into a new population using a survival mechanism. At this stage, a population of N new shape's candidates and their corresponding drags are obtained.

Finally, the previous step is repeated iteratively, for driving the evolutionary process of the genetic algorithms toward better solutions over successive generations. A number of iterations was set as a stop criterion.

It is noticed that a B-spline computation module is utilized to generate the representation of the shape of an AUV defined by its four control points. Its output is a file (.dat) that includes the points of the geometry of an AUV and the limit points of the calculation domain. This file is then processed by the ICEM journal in batch-mode to produce another file (.msh). The latter file is subsequently utilized by the FLUENT journal in batch-mode to determine the corresponding drag of the AUV. The ICEM and FLUENT journals have been developed and tested based on the aforementioned CFD modeling steps. The ICEM (FLUENT) journal refers to the script file using ICEM (FLUENT) commands. It enables automated workflow optimization without a need to manually execute each step. As an editable text file, it allows workflows to be customized to meet specific project requirements, ensuring precise control over settings and avoiding the use of default inputs without user awareness.

It is important to note that the meshes of the optimal solutions of each iteration of the optimization process were thoroughly examined during the executions of this study to ensure their compliance with the desired physics.

5 Results and discussion

5.1 Drag coefficient

Table 2 shows the optimization results obtained for the drag coefficient, showcasing significant improvements. The data reveals a remarkable 19% reduction in drag when compared to the previous numerical simulation.

Table 2 Drag of the optimized AUV

	CFD Present study	CFD Optimized AUV
Cd	0.00149	0.00121

5.2 Geometry evolution

Figure 13 demonstrates the remarkable capability of manipulating a relatively small number of control points in achieving a more suitable shape to fulfill a specific objective, such as minimizing drag. One of the key advantages of using B-splines for shaping the nose and tail of the AUV torpedo geometry is the ability to modify them without altering other design specifications, such as the length and the diameter of the underwater vehicle.

In the studies by Gao and al. [16] and Saghafi and Lavimi [19], where the design of the underwater vehicle was based on mathematical equations, the optimization process inherently resulted in changes to the overall length or diameter of the UV, as well as the positioning of its mid-section. This was in addition to modifications in the lengths of the nose and tail.

These design specifications are considered valuable and useful and could be crucial, particularly in terms of avoiding potential constraints like space occupancy.

Figure 14 illustrates a superposition of two AUV's that depicts the evolution from the original DREA shape to the optimized geometry, effectively minimizing drag.

5.3 Pressure coefficient

Figure 15 illustrates the pressure coefficients Cp in relation to the UV length, to verify the accuracy of the optimization results. The variation in Cp is significantly impacted by the shape of the nose, while the tail has a slightly smaller effect. A noticeable change in pressure distribution occurs at the tail, attributed to the nose's leading-edge shape, although the tail shape itself does not significantly alter the pressure distribution along the UV hull. However, the most optimal geometry of the UV, based on the pressure distribution, is the optimized one.

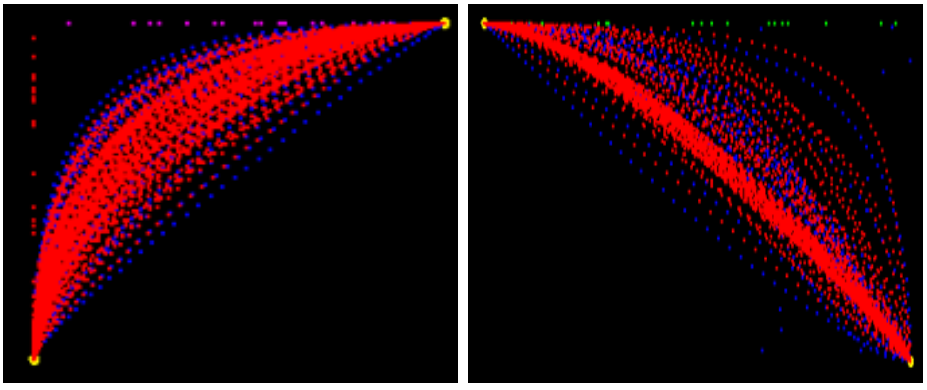

(a) Nose (b) Tail

Figure 13 Evolution of best generation's individual toward optimal solution

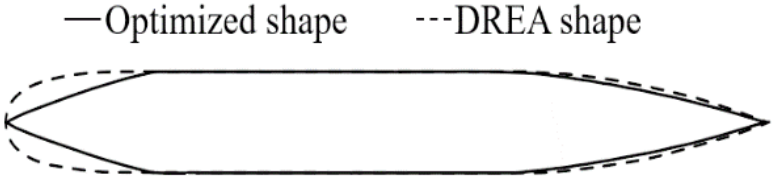

Figure 14 Superposition of original and optimized shape

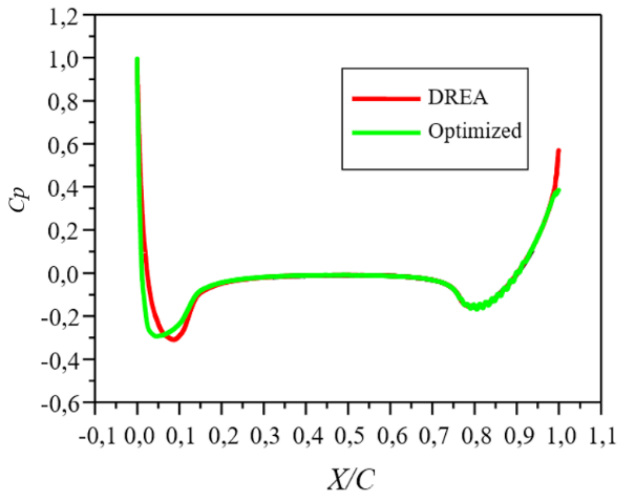

Figure 15 Pressure coefficient

5.4 Reproctubiliy

Since genetic algorithms are stochastic algorithms that operate with inherent randomness, it is important to examine the reproducibility of results when using the proposed strategy. Figure 16 demonstrates that the proposed technique exhibits a notable tendency to produce scores that are tightly clustered around the lowest values. This observation reinforces the robustness of the proposed population-based technique, which effectively avoids the potential challenge of getting trapped in local minima.

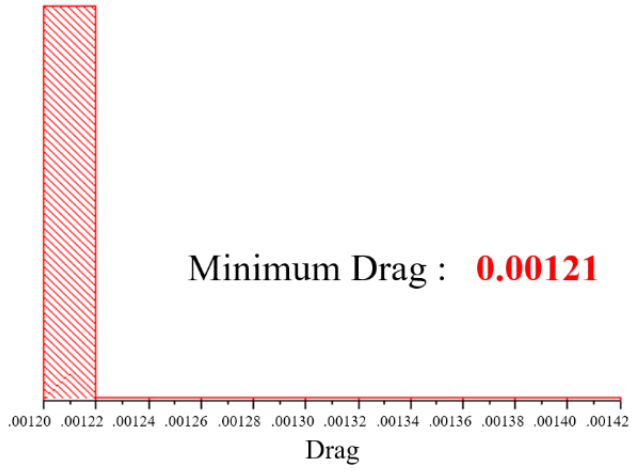

Figure 16 Reproductibility

6 Conclusion

In this study, a numerical investigation was undertaken to determine the optimal shape of a torpedo-shaped AUV based on minimum drag. The use of CFD code was imperative to set up the mesh for drag calculation. 2D steady flow using K-epsilon model was then calibrated and validated with experimental data. The proposed approach combines the use of B-spline for AUV torpedo shape construction and an adapted genetic algorithm for drag optimization.

Minimum control points where used to form the nose and the tail of the AUV where the mid-section which is cylindrical remain unchanged. The use of B-spline to represent the geometry of the AUV was efficacious. The optimization variables used to define the AUV are totally independent and decoupled from AUV characteristics such as its length and diameter. The minimum drag was obtained without modifying the dimensions of AUV's length, diameter and mid-section which can be considered as design parameters especially the mid-section.

The selected genetic algorithm technique showed its capability to efficiently converge toward the optimum. Since genetic algorithms are stochastic, a reproducibility study was conducted to emphasize its ability to repeatedly find global optimum thus drag minimum. The robustness of the presented automated optimization method resulted in a drag reduction of 19 %.

Funding: The research presented in the manuscript did not receive any external funding.

Author Contributions: Conceptualization, Data collection, Methodology, Software, Visualization, Writing original draft, Writing review & editing – Ibrahim Ayad; Supervision, Conceptualization (supporting), Writing review & editing – Benameur Hamoudi, Tahar Nateche; Writing review & editing – Mahfoudh cerdoun, Mohammed Hadj Meliani, Abdellah Mokhtari.

References

[1] Niu, H.; Adams, S.; Lee, K.; Husain, T.; Bose, N. (2009). Application of autonomous underwater vehicles in offshore petroleum industry environmental effects monitoring. Journal of Canadian Petroleum Technology, 48(5), 1515–1530. https://doi.org/10.2118/2007-116.

[2] Wenbao, G.; Xinze, L.; Lin, W.; Kejia, W.; Xinjie, X. (2021). Development of underwater vehicle's application in offshore oil and study on the key problems of anti-disturbance control. Journal of Physics: Conference Series, 1979. doi:10.1088/1742-6596/1976/1/012054.

[3] Di Ciaccio, F.; Troisi, S. (2021). Monitoring marine environments with Autonomous Underwater Vehicles: A bibliometric analysis. Results in Engineering, 9. https://doi.org/10.1016/j.rineng.2021.100205.

[4] Barker, L. D. L.; Jakuba, M. V.; Bowen, A. D.; German, C. R.; Maksym, T.; Mayer, L.; Boetius , A.; Dutrieux, P.; Whitcomb, L. L. (2021). Scientific Challenges and Present Capabilities in Underwater Robotic Vehicle Design and Navigation for Oceanographic Exploration Under-Ice. Results in Engineering, 12(16), 2588. https://doi.org/10.3390/rs12162588.

[5] Allotta, B.; Bargagliotti, S.; Botarelli, L.; Caiti, A.; Calabrò, V.; Casa, G.; Cocco, M.; Colantonio, S.; Colombo, C.; Costa, S.; Fanfani, M.; Franchi, L.; Gambogi, P.; Gualdesi, L.; La Monica, D.; Magrini, M.; Martinelli, M.; Moroni, D.; Munafò, A.; Pace, G.; Papa, C.; Pascali, M. A.; Pieri, G.; Reggiannini, M.; Righi, M.; Salvetti, O.; Tampucci, M. (2012). Thesaurus Project: Design of New Autonomous Underwater Vehicles for Documentation and Protection of Underwater Archaeological Sites. Progress in Cultural Heritage Preservation. 4th International Conference. EuroMed 2012. Lecture Notes in Computer Science, 7616. https://doi.org/10.1007/978-3-642-34234-9_50.

[6] von Oppeln-Bronikowski, N.; Zhou, M.; Bahadory, T.; de Young, B. (2021). Overview of a new Ocean Glider Navigation System: OceanGNS. Front. Mar. Sci. 8(67), 1103. doi: 10.3389/fmars.2021.671103.

[7] Hess, J. L. (1976). On the problem of shaping an axisymmetric body to obtain low drag at large Reynolds numbers. Journal of Ship Research, N°486, 51-60.

[8] Sarkar, T.; Sayer, P. G.; Fraser, S. M. (1997). A study of autonomous underwater vehicle hull forms using computational fluid dynamics. International journal for numerical methods in fluids, 25, 1301–1313. https://doi.org/10.47176/jafm.16.08.1702.

[9] Baker, C. (2004). Estimating drag forces on submarine hulls. Department of Research and Development Canada-Atlanta, National Defense. 16(8), 1515–1530. https://doi.org/10.47176/jafm.16.08.1702.

[10] Jagadeesh, P.; Murali, K. (2005). Application of low-re turbulence models for flow simulations past underwater vehicle hull forms. Journal of Naval Architecture and Marine Engineering, 2 (1), 41–54. https://doi.org/10.3329/jname.v2i1.2029.

[11] Jagadeesh, P.; Murali, K.; Idichandy,V. (2009). Experimental investigation of hydrodynamic force coefficients over AUV hull form. Ocean Engineering, 36(1), 113–118. https://doi.org/10.1016/j.oceaneng.2008.11.008.

[12] Alvarez, A.; Bertram, V.; Gualdesi, L. (2009). Hull hydrodynamic optimization of autonomous underwater vehicles operating at snorkeling depth. Ocean Engineering, 36(1), 105–112. https://doi.org/10.1016/j.oceaneng.2008.08.006.

[13] Karim, M. M.; Rahman, M. A.; Alim, M. M. (2011). Performance of SST k-ω turbulence model for computation of viscous drag of axisymmetric underwater bodies. IJE Transactions B: Applications, 24(2), 139–146.14.

[14] Alam, K.; Ray, T.; Anavatti, S. G. (2014). Design and construction of an autonomous underwater vehicle. Neurocomputing, 142, 16-29. https://doi.org/10.1016/j.neucom.2013.12.055.

[15] de Sousa, J. V. N.; de Macêdo, A. R. L.; de Amorim Junior, W. F.; de Lima, A. G. B. (2014). Numerical Analysis of Turbulent Fluid Flow and Drag Coefficient for Optimizing the AUV Hull Design. Open Journal of Fluid Dynamics, 04(3), 14. https://doi.org/110.4236/ojfd.2014.43020.

[16] Gao, T.; Wang, Y.; Pang, Y.; Cao, J. (2016). Hull shape optimization for autonomous underwater vehicles using CFD. Engineering Applications of Computational Fluid Mechanics, 10(1), 599-607. 10.1080/19942060.2016.1224735.

[17] Mostafapour, K.; Nouri, N. M.; Zeinali, M. (2018). The Effects of the Reynolds Number on the Hydrodynamics Characteristics of an AUV. Journal of Applied Fluid Mechanics, 11(2), 343-352. https://doi.org/10.47176/jafm.16.08.1702.

[18] Sedini, A.; Saidi, F.; Mokhtari, A.; Laffane, Z. (2019). Optimization and analysis of the hydrodynamic coefficients for an underwater vehicle (UV). WSEAS Transactions on Fluid Mechanics, 24, 154–161. https://doi.org/10.47176/jafm.16.08.1702.

[19] Saghafi, M.; Lavimi, R. (2020). Optimal design of nose and tail of an autonomous underwater vehicle hull to reduce drag force using numerical simulation. Proc IMechE Part M: J Engineering for the Maritime Environment, 234(1), 76–88. https://doi.org/10.1177/1475090219863191.

[20] Gertler, M. (1950). Resistance experiments on a systematic series of streamlined bodies of revolution: for application to the design of high-speed submarines. Navy Department, David W. Taylor Model Basin.

[21] Myring, D. F. (1976). A theoretical study of body drag in subcritical axisymmetric flow. Aeronautical Quarterly, 27(03), 186-194. https://doi.org/10.1017/S000192590000768X.

[22] White, N. M. (1977). A comparison between a simple drag formula and experimental drag data for bodies of revolution. David W Taylor Naval Ship Research and Development Center Bethesda MD, 77-0028. https://doi.org/10.1186/s10033-019-0360-8.

[23] Chaudhuri, A. (2021). B-spline. In Lee (Eds). Encyclopedia of Computer Graphics and Games. Springer Nature Switzerland AG 2019N. https://doi.org/10.1007/978-3-319-08234-9_359-1.

[24] William, J. G.; Richard F. R. (1974). B-spline curves and surfaces. Computer Aided Design, Academic Press. 95-126. https://doi.org/10.1016/B978-0-12-079050-0.50011-4.

[25] Ball, A. A.; Storry, D. J. T. (1988). Conditions for tangent plane continuity over recursively generated B-Spline surfaces. ACM Transactions on Graphics, 7(2), 83–102. https://doi.org/10.1145/42458.42459.

[26] Jin, Y.; Zhao, S.; Wang, Y. (2019). An optimal feed interpolator based on G2 continuous Bézier curves for high-speed machining of linear tool path. Chinese Journal of Mechanical Engineering, 32:43. https://doi.org/10.1186/s10033-019-0360-8.

[27] Huang, Q. X.; Hua, S. M.; Martin, R. R. (2005). Fast degree elevation and knot insertion for B-spline curves. Computer Aided Geometric Design, 22, 183-197. https://doi.org/10.1145/42458.42459.

[28] Mohammadi, B.; Pironneau, O. (1994). Analysis of the K-epsilon turbulence model. John Wiley and Sons.

[29] Joung, T.; Sammut, K.;He, F.; Lee, S. K. (2009). A study on the design optimization of an AUV by using computational fluid dynamic analysis. In: Proceedings of the Nineteenth International Offshore and Polar Engineering Conference, 696–702. https://doi.org/10.3329/jname.v2i1.2029.

[30] Helmaoui, M.; Saidi, F.; Laidoudi, H.; Sedini, A.; Ghenaim, A. (2020). Layout Effect of Two Autonomous Underwater Vehicles on the Hydrodynamics Performances. Ocean Engineering, 19, 47–54. https://doi.org/10.37394/23202.2020.19.7.

[31] Rahul Krishna, H.; Issac, Manoj T.; Ebenezer, D. D (2023). Numerical investigation of two-dimensional axisymmetric and three-dimensional flow simulations over a bench-

mark underwater vehicle. Physics of Fluids, 35(1): 015149. https://doi.org/10.1063/5.0134985.

[32] Pope, S. B. (2000). Turbulent Flows. Cambridge: Cambridge University Press. https://doi.org/10.1017/CBO9780511840531.

[33] Nouri, N. M.; Mostafapour, K.; Hassanpour, S. H. (2016). CFD Modeling of Wing and Body of an AUV for Estimation of Hydrodynamic Coefficients. Journal of Applied Fluid Mechanics, 9(6), 2717-2729. https://doi.org/10.47176/jafm.16.08.1702.

[34] Schmitt, L. M. (2001). Theory of genetic algorithms. Theoretical Computer Science, 259, 1–61. https://doi.org/10.47176/jafm.16.08.1702.

[35] Ying, T. (2016). GPU-based Parallel Implementation of Swarm Intelligence Algorithms. Elsevier. https://doi.org/10.1016/C2015-0-02468-6.

[36] Garden, R. W.; Engelbrecht, A. P. (2014). Analysis and classification of optimization benchmark functions and benchmark suites. IEEE Congress on Evolutionary Computation (CEC), 1641–1649. Doi: 10.1109/CEC.2014.6900240.